DRAFT

How Slight Solidification Rate Variations within Cast Plate Affect Mechanical Response: A Study on As-Cast A356 Alloy with Cu Addition

Di Giovanni, Maria Teresa
Università degli Studi di Parma - University of Parma
Cerri, Emanuela
Università degli Studi di Parma - University of Parma
Saito, Takeshi
Norsk Hydro ASA - Norsk Hydro ASA
Akhtar, Shahid
Norsk Hydro ASA - Norsk Hydro ASA
Åsholt, Petter
Norsk Hydro ASA - Norsk Hydro ASA
Li, Yanjun
Institutt for materialteknologi - Norges teknisk-naturvitenskapelige universitet
Di Sabatino Lundberg, Marisa
Institutt for materialteknologi - Norges teknisk-naturvitenskapelige universitet

INTRODUCTION

Alloy composition and cooling conditions during solidification play a key role towards the mechanical properties of Al-Si cast alloys. The cooling rate controls the coarseness of the microstructure including: i) the Secondary Dendrite Arm Spacing, SDAS, which is often used as a measure of the coarseness of the microstructure, and thus as measure of the mechanical response; and ii) the fraction, size, shape and distribution of Si-particles and intermetallic phases in the α-Al phase [1, 2]. Si particles, providing inhomogeneity in the α-Al matrix, act as the principal source of stress concentrators [3,4,5,6], therefore, industrial castings are regularly modified by Sr additions. A change of the eutectic Si particles from needle-like into fibrous morphology will improve the ductility of the material.

Among the Al-Si foundry alloys, the most commonly used are the A356 and A357, where, besides Si, Mg and Cu are the major alloying elements due to their strengthening ability by precipitating metastable precipitates under age-hardening treatment. Precipitation mechanisms are rather complicated and several phases such as β (Mg_2Si), θ ($CuAl_2$), S ($CuMgAl_2$) or Q ($Cu_2Mg_8Si_6Al_5$) in metastable ~~situation~~ may exist [7,8]. Numerous investigations confirm that the strength of this class of material is achieved at the expense of ductility [9,10]. Seifeddine et al. [1,11] found Cu and Mg promote the formation of bands of coarse Si particles, ~~as they~~ ~~also~~ enlarge the solidification interval, ~~leading to an~~ increasing the risk for shrinkage porosity, thus compromising the ductility. Literature correlated the plastic deformation behavior as function of factors such as ~~whether the~~ Cu and Mg ~~are~~ found as coarse intermetallic compounds, the level of Cu and Mg in solid solution, or ~~if~~ Cu and Mg ~~are~~ ~~found as~~ GP zones formed at room temperature and/or as precipitates due to a post solidification treatment. A recent study demonstrated that high Cu concentrations in the Al-Si-Cu-Mg-Fe system can refine, and hence counteract, Fe-bearing intermetallics [12].

Whereas the most pertinent literature focuses on the influence of a single variable on the mechanical properties of cast Al-Si-Mg alloy, the present study proposes a comprehensive study on the influences of different factors on the mehcanicale properties of an A356 foundry alloy. The two aspects of SDAS and Cu additions were correlated in series and parallel. Samples were selected from 3 different positions in the cast, offering 30, 35, 40 SDAS variant. Cu was added to the cast to reach 3 target concentrations, i.e. 0, 0.5, and 1 % wt. In addition to the above mentioned issues, Si particles size and distribution were analyzed over the 9 (3x3) different conditions, and the influence of Cu on the Cu/Mg/Fe-rich intermetallic phases was examined by SEM and EDS spectra.

Alloy	Si	Mg	Fe	Cu	Ti	Al	Code
A356	6.624	0.216	0.086	0.006	0.103	bal.	Cu0
A356 + 0.5 wt% Cu	6.587	0.258	0.082	0.454	0.105	bal.	Cu0.5
A356 + 1 wt% Cu	6.915	0.262	0.091	0.983	0.086	bal.	Cu1

MATERIALS AND METHODS

Material

The materials used in this study were produced by Hydro Aluminum in Norway. Commercial Sr-modified A356 alloy was melted in a boron-nitride coated clay-graphite crucible at 1023 K (750 °C), and grain refined by means of Al-5Ti-1B master alloy additions. Cu was added to the melt in form of pure cupper grains according to the targeted nominal concentrations of 0, 0.5 and 1 wt. %. The molten metal was successively stirred and allowed to settle for 30 min to ensure complete dissolution. The alloys were then degassed with argon gas for 5 min just prior to be poured in a ~~cupper~~ mold of 65 mm x 103 mm x 40 mm. The temperature of the die was kept at 323 K (50 °C) during the casting trials. Samples from the three different melts were taken and analyzed by optical emission spectroscopy (OES). The chemical composition of the alloys is given in Table I.

Table I.

Chemical composition (wt%) of A356 reference alloy and Cu-containing alloys as measured by OES and their classification.

Thermal Analysis

The experimental setup for thermal analysis measurements is described as follows: a graphite crucible was preheated at 1023 K (750°C) and placed on top of the skimmed and thoroughly stirred melt. After the temperatures of crucible and melt had reached equilibrium, samples were taken by submerging the graphite crucibles into the melt. The filled crucibles were then placed on Fiberfrax board and a K-type thermocouple was lowered into the melt. The thermocouple tip was placed in the center of the sample. A Campbell logger (Campbell Scientific, Inc., USA) recorded the temperature-time curve at a frequency of 50 Hz. Prior to and after a measurement the range of eventual thermocouple drift was checked against high purity aluminum (Al5N grade) assuming a solidus temperature of 1410 K (660°C).

Mechanical tests

Tensile tests were performed at room temperature, using an MTS 810 Universal Testing Machine . The crosshead speed was 1mm/min ~~and the applied load was restricted to 40 Knm~~. The specimens,

with a gauge length of 7 mm , cross area of 4 mm x 4 mm were cut from three different positions in the ingot: at 4 mm from ~~the cast bottom skin, at~~ 8 mm, and 12 mm, respectively referred as Bottom, Center and Top (as shown in Figure 1). Stress-strain curves were obtained by attaching a knife-edge extensometer to the specimens' gauge length and the tensile properties, such as yield strength, ultimate tensile strength and percentage elongation ($Rp_{0.2}$, UTS and A%, respectively) were determined. Vickers micro hardness tests (HV) were performed at the Bottom (B), Center (C) and Top (T) of the cast ingots at a load of 300 g and a dwell time of 15 s, according to UNI EN ISO 6507 specification. Further hardness examinations were conducted by means Rockwell hardness measurements, with a load of 60 kgf, and 1/16'' ball intender (HRF) according to UNI EN ISO 6508-2 specification.

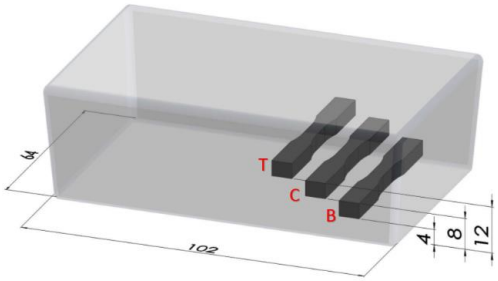

Fig.1 – Specimen cutting position. Respectively, B: Bottom specimen, C: center specimen and T: top specimen (values are given in mm).

Microstructure

Samples for microstructural investigations were cut from the tensile specimens, embedded in phenolic resin and prepared using standard grinding and polishing procedures. Microstructure analyses were performed using a LEICA DMi8 polarized light optical microscope (OM) equipped with a LASX image analysis program. SDAS measurements were performed using the line intercept method. Secondary phases were investigated with a ZEISS ULTRA 55 field emission scanning electron microscopy (FE-SEM) and identified through energy dispersive X-ray spectroscopy (EDS). A statistic study on the Si particles equivalent diameter (ED) and surface area (SA) distribution has been also carried out. In order to analyze the particles, a specific threshold has been defined. Pixel color ranges have been restricted to the scale of light grey corresponding to Si particles. ED distributions were detected by using a 100X objective lens whereas a 20x objective lent has been used to identify a representative Si-particles surface area distribution over the three interested zone: B, C, T. Secondary phases were investigated with a ZEISS ULTRA 55 field emission scanning electron microscopy (FE-SEM) and identified through energy dispersive X-ray spectroscopy (EDS).

RESULTS / DISCUSSION

Thermal Analysis

Solidification curves and associated slopes for the Al-Si-Mg reference alloy and Cu-containing alloys are given in Fig. 2. Two reactions, i.e. the nucleation and growth of the α-Al (highest T inflection point) and of the Si eutectic (lower~~s~~ T inflection point), can be easily identified.

Nucleation temperature of primary aluminum dendrites (T_α) shifts to a lower temperature with increasing Cu content. According to Arnberg [13] and Bäckerud [14] a commercial unmodified A356 alloy, with a cooling rate of 1.1 K/s before solidification, starts with precipitation of α-Al at 610°C. This temperatures varies within the range of 608-615°C with different cooling rates. Whereas the Cu0, A356 reference alloy of our ~~case of~~ study, shows that formation and growth of primary α-Al dendrites begins at 622 ± 1°C (average of at least 3 repeated measurements). The shift observed, is mainly imputable to the presence of Ti_2B, well known as excellent grain refiner for this class of material. When it comes to Cu-rich variants, the grain refiner seems to deflate his effect and, as result, Cu0.5 and Cu1 dendritic networks start to grow at the temperatures of 618 ± 1°C and 615°C ± 2°C, respectively. Temperatures ranges, bearing the presence of grain refining, agree with those present by Mackay [15] suggesting for an A356 alloy with high Cu content (0.61 wt%) the temperature of formation and growth of primary α-Al dendrites at 612°C. Approaching the eutectic transformation, we can observe similar trends and thus, as expected, the eutectic transformation of Cu0 variant occurs at 578 ± 1°C. The influence of Cu is more prominent in this reaction as the Cu0.5 and Cu1 T_{eu} decrease sensibly by 18°C. The general trend ~~in the data shown in Fig.2~~ for cooling rate is that an increase tends to depress eutectic reaction start temperatures.

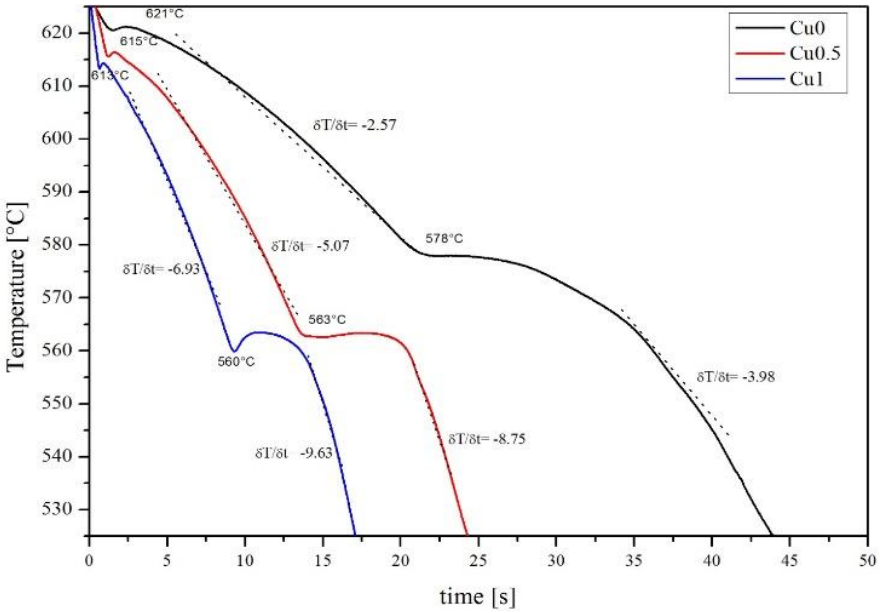

Fig.2. *Cooling curves and associated first derivative for Cu-free A356 variant in black, Cu0.5 variant in red and Cu1 in blue.*

Mechanical Properties

Fig.3 summarizes room temperature tensile curves of the three alloys as a function of Cu-content (a,b,c in Fig.3) and specimen cutting position (d,e,f in Fig.3).

Curves a,b,c clearly evidence improvement in strength with increasing Cu content, for the three B,C, and T specimens. In parallel, the tendency observed in in Fig.3 d,e,f revealed how the specimen cutting position (hence, cooling rate and microstructure) strongly influences the mechanical properties leading to an enhancement in strength by approximately 10% and 20% for the Cu-free and the Cu-containing alloys, respectively, moving from the top to the bottom in the cast. Compar-

ing the curves d, e, and f in Fig.3, it is evident that elongation (A%) decrease with increasing Cu-content. Nevertheless, Cu0.5 and Cu1 associated elongations~~, offer A% values~~ ranging between 6-9% well above ~~as-cast~~ literature average [16]. (Other consideration to add, e.g. towards elongation…)

The two phenomena might be related to the solidification mechanism and/or microstructural features. In this light, both these aspects will be investigated.

A convenient and widely used measure of the effect of solidification conditions on dendrite structure is the *secondary dendrite arm spacing* (SDAS). The SDAS, which is the linear distance between two secondary aluminum dendrites (arms), was determined via the mean linear intercept (MLI) method.

Fig. 4 reveals how cooling conditions are strongly subjected to mold skin distance, even though the region interested is restricted to a distance of 12 mm (refer Figure A). Top SDAS measurements evidenced an increase by 50% for the Cu0 and Cu1, and by 25% for the Cu0.5 case, as compared to the Bottom. Results are consistent with material tensile response observed in Fig.3.

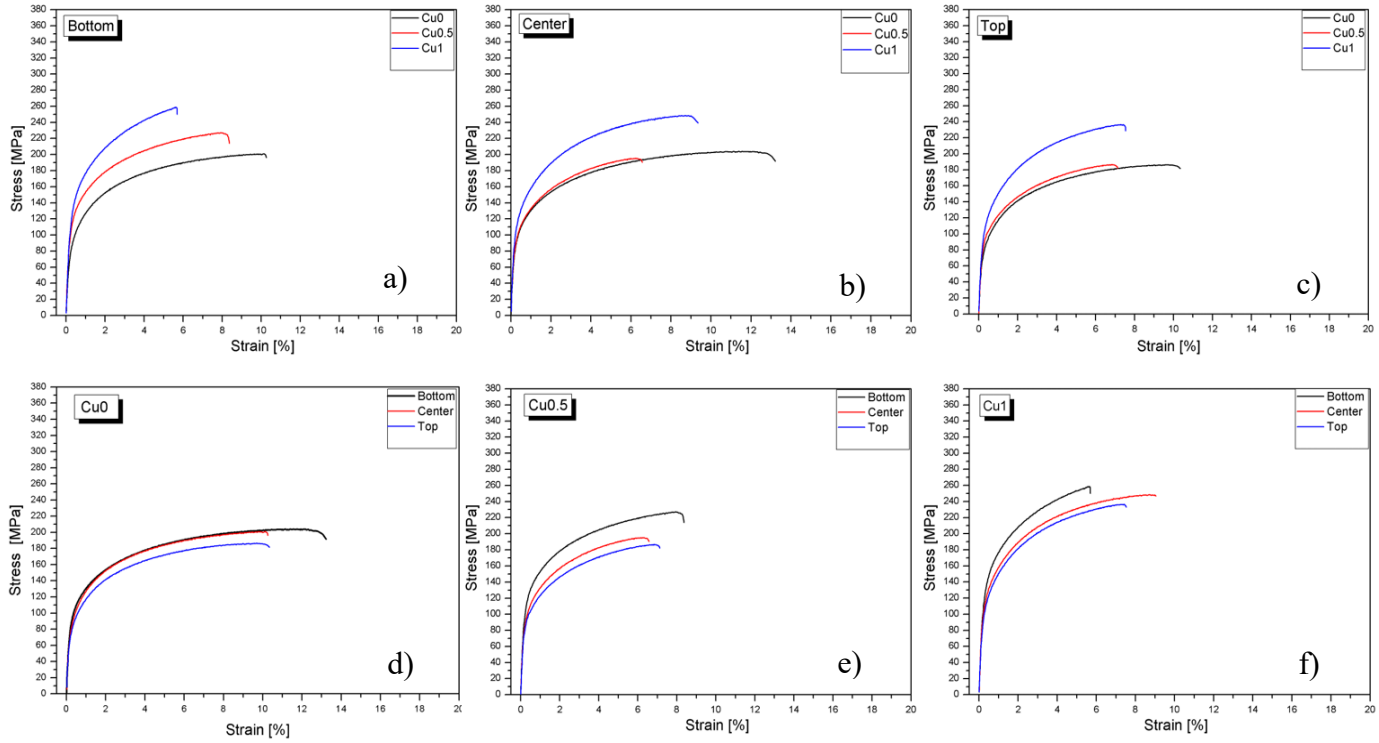

Fig. 3. Tensile strength-strain curves of the three investigated alloys as a function of both Cu-content (a,b,c) and specimen cutting position (d,f,g).

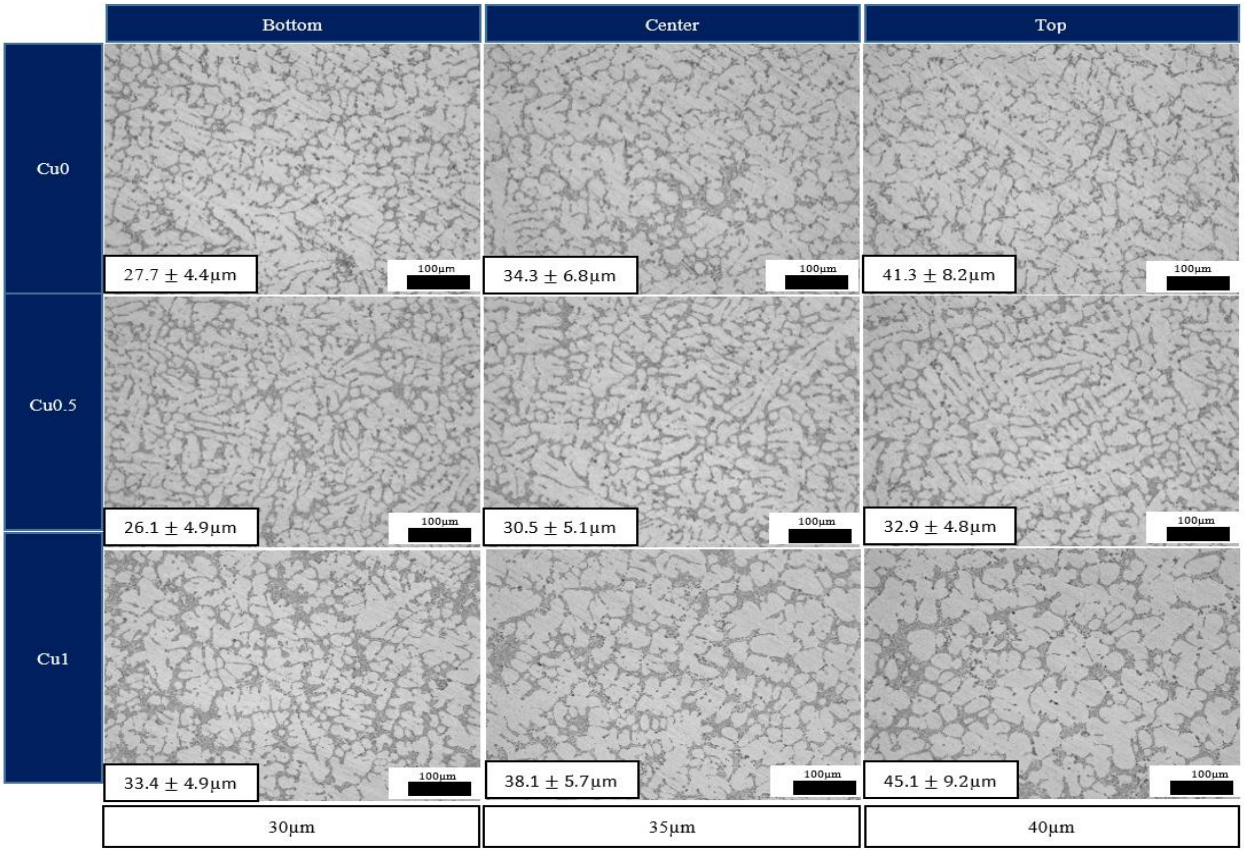

Fig.4 Optical micrographs and SDAS measurements as function of Cu-content and ~~as~~ specimen cutting position; (a)-(c) depict the microstructure of the Cu-free alloy; (d)-(f) of the 0.5% Cu alloy and (g)-(i) of the 1% Cu alloy with SDAS ranging from 30 up ~ 40 µm.

To further address the influences of both the Cu-content and cooling rate, hardness measurements were also conducted.. It is a conventional wisdom that hardness correlates linearly to Ultimate Tensile Strength through the empirical (although theoretically explained) equation H=UTS/k, where k is a constant that depends on the hardness scale / type of measurement and on the material. Despite these assumptions, HV and HRF measurements do not reveal a clear enhancement in hardness, moving from bottom to top, as expected with reference to the tensile properties, shown in Fig.3, whereas, the influence of Cu addition is prominent in increasing the hardness response of this alloy. It is worth nothing how hardness development, straight follows the Cu content. At this point, tensile properties variance, resulting comparing B and T sample (d, e and f, in Fig.3), has been interpreted trough SDAS measurements (Fig.4), and the 10 µm shift, albeit its impressive effect on a small scale (12 mm), seem not to be the sole cause behind the tensile behavior. Furthermore, hardness evolution, did not confirm the tensile variation nay, focusing on the HRF measures, it is possible to observe a slight increment in hardness, moving from the B to the T, in evident contrast to the tensile response evolution.

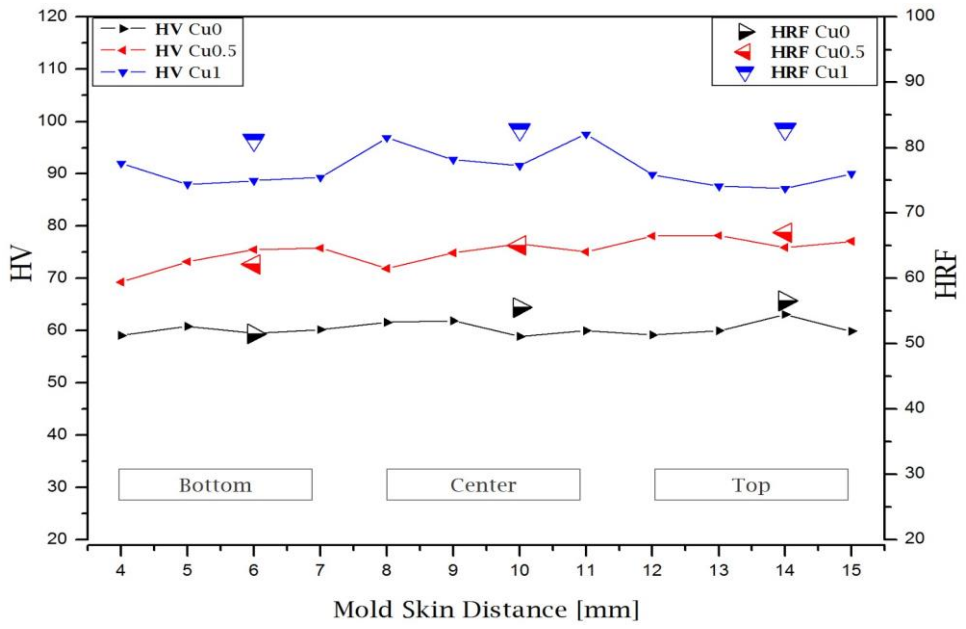

Fig.5 Cast ingot hardness profile. Vickers Microhardness scale on the left, Rockwell Hardness scale on the right.

Microstructural Investigation

In order to understand deeply how the observed shift in strength is correlate to the hardeness response, microstructural features have been investigated and in particular, Si particles equivalent diameter distribution and Si particles % areas values have been presented in Fig. 6.

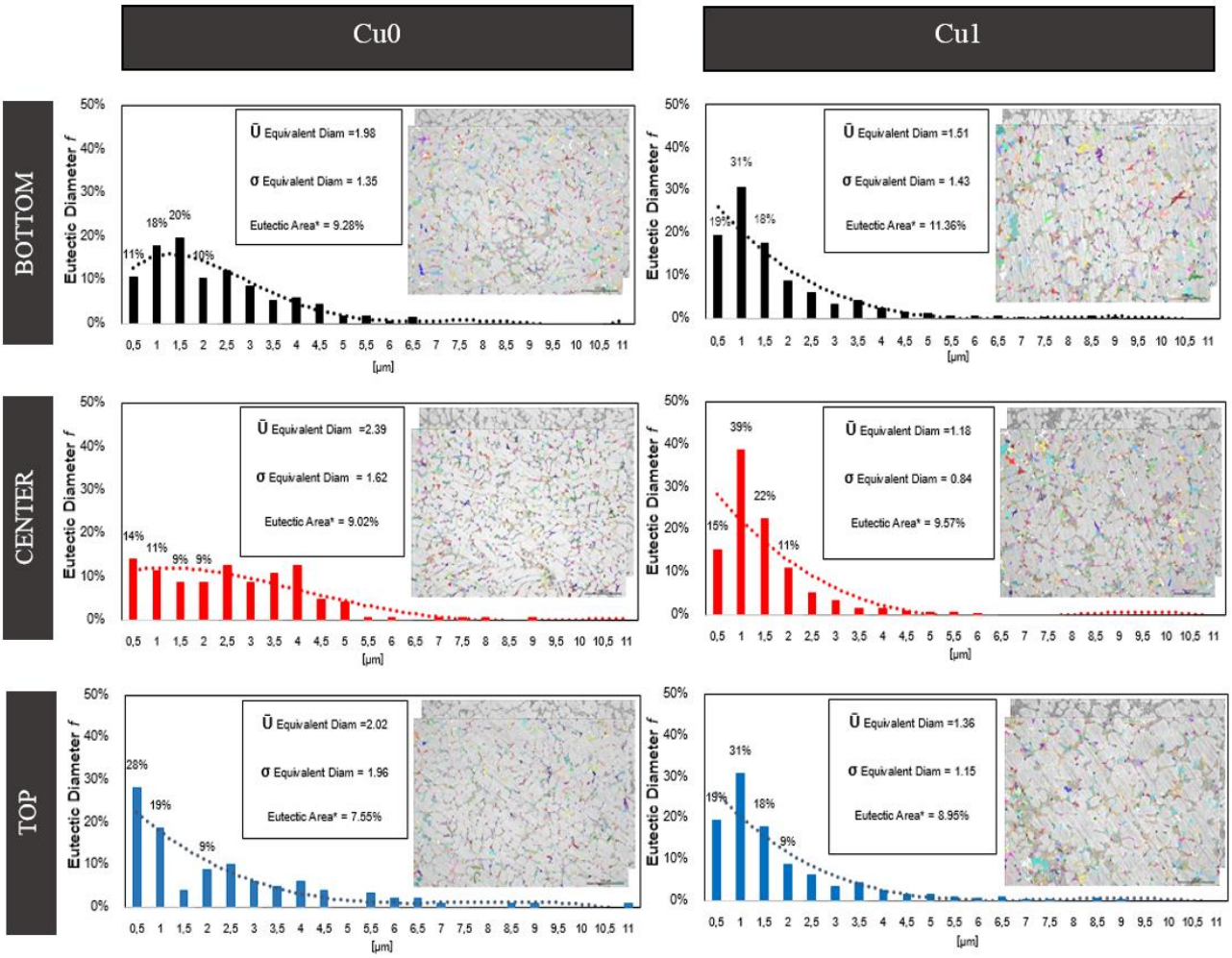

Fig. 6 – Distribution of the Eutectict Si particles' equivalent diameter. Comparison between Cu-free and Cu-containing alloys (1 wt% Cu) in the three bottom, center and specimen cutting position.

The distribution curves, obtained using chi-square goodness-of-fit test have been plotted for representative alloys which encompass Cu-free and 1%wt Cu-containing alloys for the three Bottom, Center and Top specimen cutting position. The results revealed that Sr-modification strongly affects the Si particles size (in particular the effect is more pronounce in the Cu1 case) as compared to the unmodified alloys [17].

At first blush, Cu0's equivalent diameter (ED) distributions appear to be flatter if compared to Cu1 distributions, to the Cu addition.

On the other hand, frequency differences longitudinally across the different position (a,c,e and b,d,f) highlight a feeble, but anyway significant, lowering of the distribution curve, suggesting an overall decrease in the Si particles ED size moving from the Top to the bottom position. Focusing on the macro-scale (20x Leica DMi8 objective lens), Si particles surface area has been identified over the

three interested zone: B, C, T.

Measurements show~~n~~ eutectic particles surface area (A%) to be denser ~~in~~ the bottom as compare to the top, and in parallel show~~n~~ Si –particles to be denser in the Cu-containing alloy.

Intermetallic analysis

Representative Backscattered electron (BSE) images and EDS spectra of the Cu-containing phases are presented in Fig.7. For the sake of brevity, only the as cast Cu1 BSE micrographs are reported. Since heavy elements (high atomic number) backscatter electrons more strongly than light elements (low atomic number)~~, and thus~~ appear brighter in the image, BSE are used to detect contrast between areas with different chemical compositions. As a matter of fact, Cu-bearing phases appear in white contrast - are found in different morphologies, resulting after Al-Si eutectic reaction. The θ-Al_2Cu phase, with high Cu content ~ 30% (b_2 and c_1 in Fig.7), usually coexists with other eutectic phases but it forms independently in the interdendritic region as well. It has more rounded blocky-type morphology and sometimes appears as many pockets connected to each other. The average size of this phase starts from 5 μm and goes down to 1μm. Other high-Cu content features are identified in this work as quaternary Al-Mg-Si-Cu phases (a1), and beside the at% Cu content measured by EDS, they are discernible thanks to the strong white contrast. Moreover, a particular rounded/spherical fine ternary eutectic feature, named as Al-$Al_x(SiCu)_2Mg$, was frequently observed, in both SEM and OM micrographs (b_1 in Fig.7 and b,d in Fig.9). Due to its morphology and its color contrast response (dark gray BSE, light gray OP), the quaternary Al-Mg-Si-Cu, could be easily address to the Q-phase, largely investigated by [18,19,20] ~~N~~notwithstanding, based on current EDS (repeated over 5 enchants) results, these gray intermetallics had been speculated to follow the $Al_x(MgSi)_3Cu$ stechiometry (a3,c2 in Fig.7 and b,c,d in Fig.9). A summary of all the identified phases is given in Table II.

Figures 8-a through 8-c show the well-known Fe-rich β phases. The β-platelets (light gray) appeared to be the main nucleation sites for the eutectic Si and Cu-rich phase (white), where both the phases are found to form at 525°C [21].

In conclusion, a macro overview of the Cu1 as cast microstructure is presented in Fig.9. The rounded eutectic phase is found in the middle of the a-grains, whereas both eutectic and blocky forms of the CuAl2 phase were observed in the interdendritic channels, or combined with the β -phase.

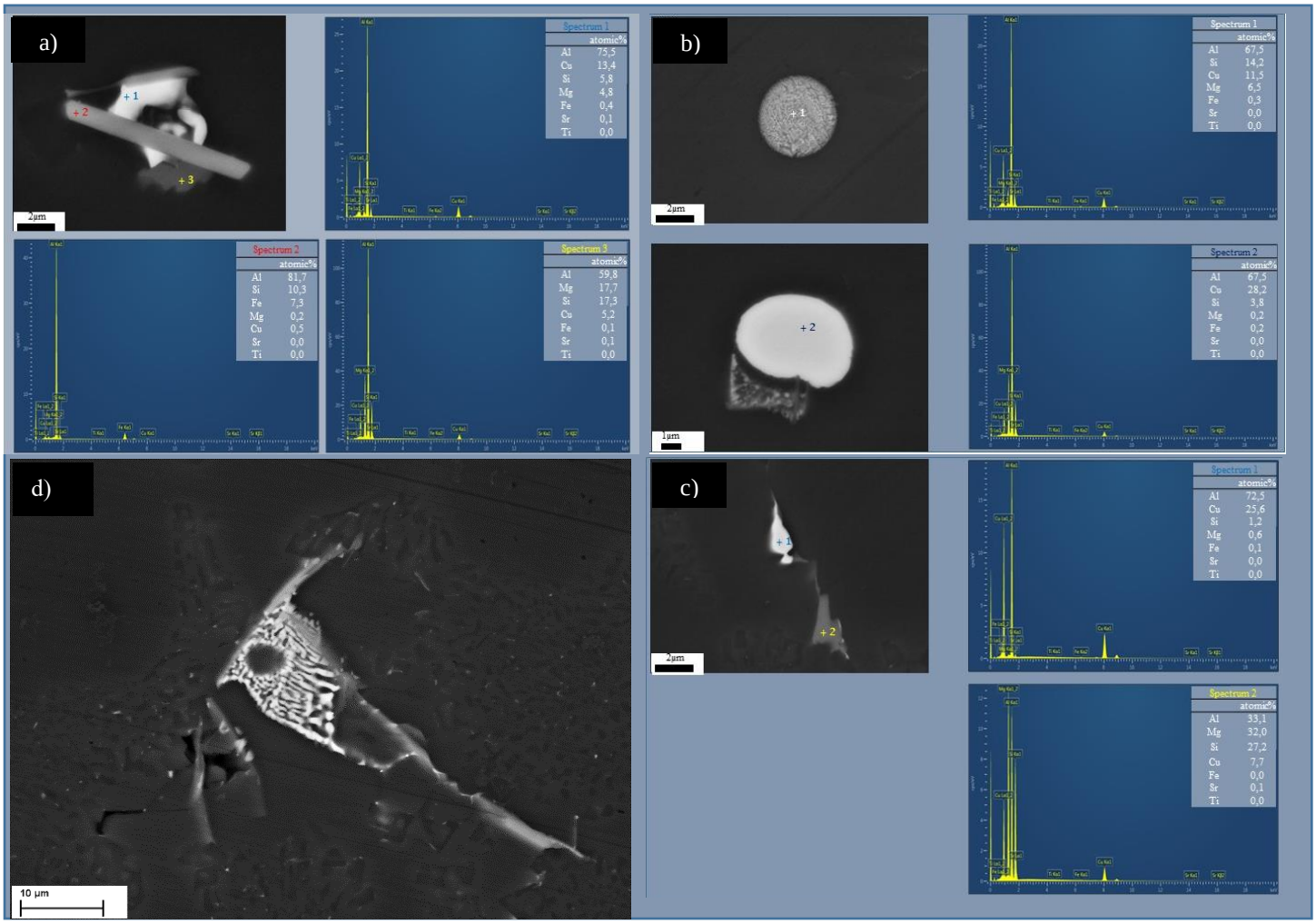

Fig.7 BSE images of some intermetallic phases detected in the Cu-containing alloy (Cu1), in the as cast condition. EDS measurements indicate the nature of the intermetallic compound as Al_2Cu, ß-Al_5FeSi and Cu/Mg bearing intermetallics.

Table II
Composition ranges of some intermetallic phases measured by semi-quantitative EDS.

	Composition in (atomic%)						
Phase	**Al**	**Si**	**Mg**	**Fe**	**Cu**	**Sr**	**Ti**
Al_2Cu (2b,1c)	67.51 - 74.3	1.24 - 3.83	0.22 - 1.76	0.04 - 0.18	22.19 - 28.21	0.0- 0.04	0.0- 0.04
ß-Al_5FeSi (2a)	63.98 - 74.56	17.13 - 22.18	0.16 - 0.45	7.6 - 12.88	0.47 - 0.53	0.0 - 0.03	0.0 - 0.02
π-$Al_8Mg_3FeSi_6$	68.07 - 75.8	17.0 - 19.81	9.04 - 14.9	3.05 - 4.6	-	0.0 - 0.01	0.0 - 0.02
? $Al_x(MgSi)_3Cu$ (3a,2c)	33.08 - 59.81	17.3 - 27.19	17.66 - 31.97	0.01 - 0.06	5.15 - 7.67	0.03 - 0.09	0.0 - 0.0
? Al- $Al_x(SiCu)_2Mg$(1b)	62.74 - 68.48	13.35 - 19.81	6.49 - 8.57	0.13 - 0.53	9.47 - 13.07	0.04 - 0.07	0.01- 0.04
? Al5MgSiCu$_3$ (1a)	75.45 - 82.42	4.23 - 5.81	3.02 - 4.8	0.04 - 0.45	9.11- 13.43	0.01 - 0.09	0.0 - 0.02

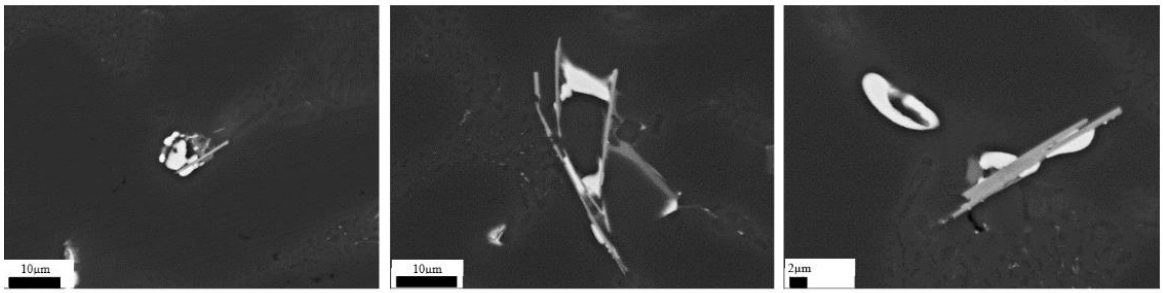

Fig .8- BSE images, showing Cu-rich intermetallics (in white) coupled with Fe-rich β phases (light gray).

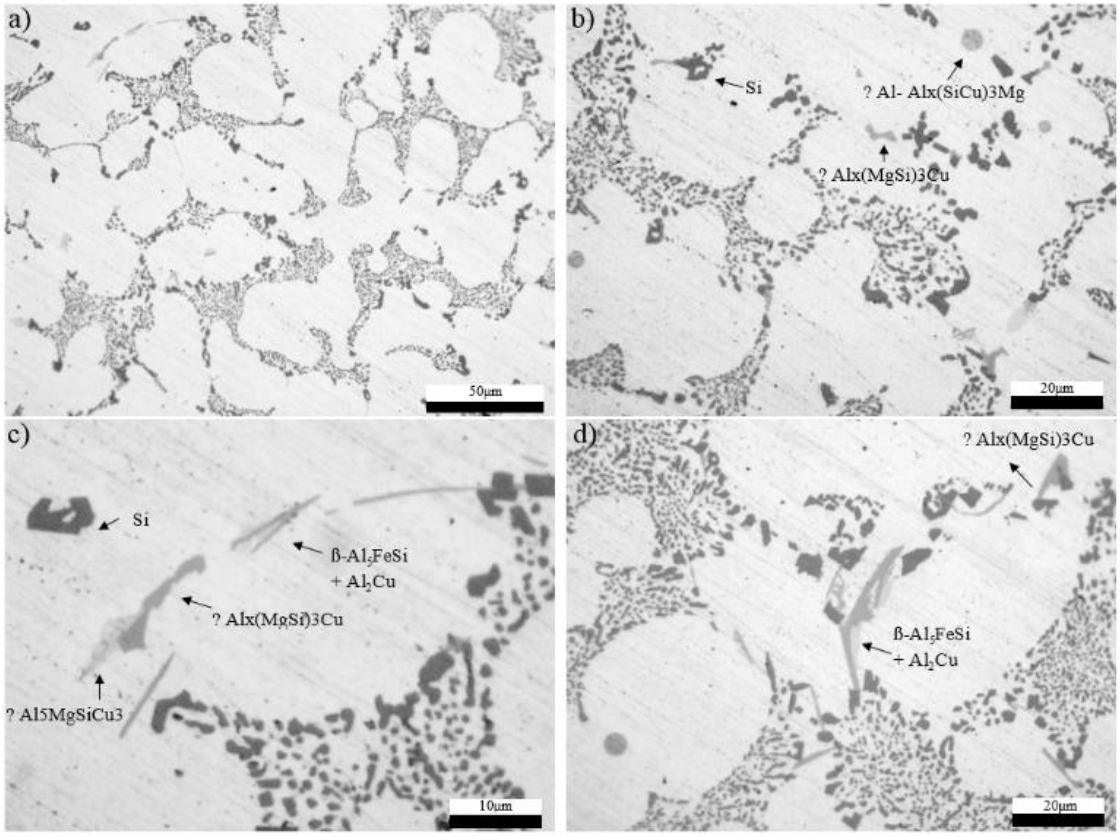

Fig.9 Optical micrographs of the Cu-Containing alloy (Cu1) where Fe-rich and Mg-/Cu-bearing phases are found as companion to the Si eutectic.

DISCUSSION/ (CONCLUSION)

Tensile curves, presented in Fig. 3, highlighted two main trends: 1) improvement in strength with increasing Cu content, for the three B, C, and T specimens; and 2) a parallel enhancement in strength moving from the top to the bottom in the cast for the three alloys. Moreover, it is important to stress how the presence of Cu did not correspondingly affect ductility, contrary to previous findings [16]. Therefore, in order to address the influence of solidification structure on the strengthening mechanism, both SDAS and hardness measurements were performed. Although SDAS measurement confirmed the shift observed in tensile strength, the ~~slight µm~~ variations appeared to be too poor to justify the trend. On the other side, hardness measurements ~~only~~ approved the enhancement in strength with increasing Cu-content, without offering a remarkable support in the understanding the alloys tensile behavior moving from the B to the T.

The alloys investigated consist of a soft, low E matrix and hard, eutectic Si particles and high E intermetallics. Similar to a composite material, the stiffer particles generally reinforced the matrix by bearing a larger proportion of the applied load [22].

Si particles ED distributions, indicated a decrease in particles size with the increase of Cu-content, even though values might be compromised by the higher Sr-content in the Cu-containing alloys, resulted after the casting. Besides this, focusing on macro properties, we found out a relevant tendency which see eutectic particles A% to be denser in the bottom, as compare to the top, and in parallel see Si –particles to be denser in the Cu-containing alloys, as compared to the Cu-free case.

Once analyzed Si particles, also the intermetallics nature has been investigated. Over 4 different Cu-bearing phase had been detected, with a Cu content ranging from ~30 to ~ 7 at%~~. Where~~ the quaternary phases (Al-Mg-Si-Cu) were found to be associated the Si particles, the θ-Al_2Cu were found to be coupled with brittle ß-Al_5SiFe phases.

Assuming that the presence of Si particles is associated to the presence of Si-/Mg-/Cu- rich intermetallics, the larger is the eutectic area the larger is the intermetallics Area. As a result, the bottom is strengthened at the expense of the α-Al matrix S.S.S., impoverished by metastable Si, Mg and Cu atoms thus not exerting a significant hardening role.

As far the ductility is concerned, besides the small Si particle size, and the excellent Sr-modification capable to counteract the fracture crack concentered load, it is worth noting how the stress concentration interesting brittle phase could might be recovered thanks to the co-existence of a coupled ductile phase. As occur for the brittle β phases, often detected to be coupled with Cu-rich phases

Acknowledgements

…

References:

1. http://dx.doi.org/10.4236/msa.2013.43020
2. DOI: 10.1016/j.jmatprotec.2004.04.302
3. Wang Q. G., Casaeres C. H., Grifhits J R.'' *Damage by eutectic particle cracking in aluminum casting alloys A356/357 ''.* Metallurgical and Materials Transactions A, 2003, 34(12): 2901−2912.
4. Fadavi I., Boostani A., Tamanthas S.,'' *Fracture behavior of thixoformed A356 alloy produced by SIMA processAlloys and Compounds''* 2009, 481(1−2): 220−227.
5. C. Caceres, I. L. Svensson and J. Taylor, "Strength-Duc-tility Behaviour of Al-Si-Cu-Mg Casting Alloys in T6 Temper," *International Journal of Cast Metals Research,* Vol. 15, No. 5, 2003, pp. 531-543.
6. S. Seifeddine and I. L. Svensson, "The Effect of Cooling Conditions and Variation of Alloying Elements on the Microstructural and Mechanical Properties of Al-7%Si Cast Alloys," *Giessereiforschung,* Vol. 58, No. 3, 2006, pp. 50-54.
7. Hossain, Abul, and ASW Kurny. "Effects of Strain Rate on Tensile Properties and Fracture Behavior of Al-Si-Mg Cast Alloys with Cu Contents." *Materials Science and Metallurgy Engineering* 1.2 (2013): 27-30
8. Barlow, I.C., Rainforth, W.M. and Jones, H., "The role of silicon in the formation of the (Al5Cu6Mg2) r phase in Al–Cu–Mg alloys", *J Mater Sci.* 35, 1413-1418, 2000.
9. Shabestari, S.G. and Moemeni, H., "Effect of copper and solidification conditions on the microstructure and mechanical properties of Al-Si-Mg alloys", *J. materials Processing Technology,* 153-154, 193-198, 2004.
10. Jin Man, Jing., Li., and Shao Guang, Jie., "The effects of Cu addition on the microstructure and thermal stability of an Al-Mg-Si alloy", *Journal of alloys and Compounds,* 437, 146, 200
11. A. L. Dons, G. Heiberg, J. Voje, J. S. Maeland, J. O. Loland and A. Prestmo, "On the Effect of Additions of Cu and Mg on the Ductility of AlSi Foundry Alloys Cast with a Cooling Rate of Approximately 3 K/s," *Materials Science and Engineering A,* Vol. 413, 2005, pp. 561-566. doi:10.1016/j.msea.2005.09.053
12. DOI: 10.1007/s11661-015-2808-5
13. L. *Arnberg*, L. Bäckerud. *Solidification Characteristics of Aluminum Alloys.* Vol. 3: Dendrite Coherency, Des Plaines, Illinois AFS, 1996
14. L. Bäckerud, G.Chai and J.Tamminen, Solidification Characteristic of Aluminum Alloys.Volume 2: Foundry Alloys, 1990, Stockholm,Sweden: AFS/SkanAluminium.
15. Lu, H. T., Wang, L. C. and Kung, S. K., "Grain Refining in A356 Alloys, J. Chinese Foundrymen's Association, Vol. 29, pp. 10-18 (June, 1981). http://dx.doi.org/10.1080/13640461.1998.11819241
16. Studies on the microstructure and mechanical properties of A356alloy with minor additions of copper and magnesium.S.A. Kori, M.S. Prabhudev and T.M. Chandrashekharaiah. Vol. 62, Issues 4-5, August-October 2009, pp. 353-356. Transactions of The Indian Institute of Metals.
17. Q.G. WANG, Metall. Mater. Trans. A, (2003), vol. 34A, p. 2887
18. http://dx.doi.org/10.1016/j.msea.2014.10.080
19. M. Murayama, K. Hono. Acta Mater., 47 (1999), pp. 1537–1548

20. G. Sha, H. Möller, W.E. Stumpf, J.H. Xia, G. Govender, S.P. Ringer. Acta Mater., 60 (2012), pp. 692–701
21. N. Tenekedjiev, H. Mulazimoglu, B. Closset, and J. Gruzleski, in Microstructures and Thermal Analysis of StrontiumTreated Aluminium-Silicon Alloys, pp. 32–52, American Foundrymen's Society, Des Plaines, IL (1995)
22. DOI: 10.1016/j.msea.2014.05.059